

Role of Si Minor Addition on Glass Formation and Flow Stress Characteristics of a Zr-Based Metallic Glass

Indah Raya^a, Tzu-Chia Chen^{b*} , Sigiet Haryo Pranoto^c, A. Surendar^{d*} ,

Anatolij Sergeevich Utyuzh^e, Samaher Al-Janabi^f, Ayad F. Alkaim^g, Nguyen Tan Danh^g,

Yasser Fakri Mustafa^h

^aChemistry Department, Faculty Mathematics and Natural Science, Hasanuddin University, Makassar, South Sulawesi 90245, Indonesia

^bDhurakij Pundit University, Bangkok 10210, Thailand.

^cUniversitas Muhammadiyah Kalimantan Timur, Faculty of Science and Technology, Department of Mechanical Engineering, Samarinda 75124, Indonesia.

^dSaveetha institute of medical and technical sciences, Chennai, India.

^eSechenov First Moscow State Medical University, Moscow, Russia.

^fUniversity of Babylon, College of science for women, Iraq.

^gFPT University, IT department, Vietnam.

^hUniversity of Mosul, College of Pharmacy, Department of Pharmaceutical Chemistry, Mosul-41001, Iraq.

Received: May 24, 2021; Revised: August 03, 2021; Accepted: August 05, 2021

The characterization of strain rate effects near glass transition temperature (T_g) gives important information on flow behavior of metallic glasses (MGs). For this purpose, the tensile strain rate jump test was carried out near glass transition temperature to evaluate the flow behaviors of ZrCoAl(Si) MG ribbons. The primary thermal analyses showed that the Si minor addition into the ZrCoAl alloy leads to the betterment of thermal stability and the glass forming ability (GFA), correlated with the small size of Si atoms and subsequent formation of denser atomic clusters and thermodynamically liquid stabilization in the system. The tensile strain rate jump test indicated that minor adding of Si element decreases the sensitivity of glassy alloy to the flow stress and improves the stability of amorphous structure under increase in the strain rate and applied temperature. It was also observed that the viscosity behavior is more stable with the increase of the strain rate and temperature in the Si-added sample, implying the high capability of viscoplastic response in this state.

Keywords: *Metallic glass, flow stress, thermal stability, deformation.*

1. Introduction

As a distinct classification of metallic alloys, metallic glasses (MGs) possess unique properties such as high elastic limit, good wear behavior, superior yield strength and excellent corrosion resistance¹⁻³. However, poor room-temperature ductility of MGs under tensile loading is a big challenge to apply them in engineering structures^{4,5}. Several works have been done to identify mechanism of flow stress behavior of MGs under tensile loading and few studies have succeeded to improve tensile flow characteristics in amorphous alloys⁶⁻⁸. Tensile loading sensitivity is so high that even the MG composites are exposed to the brittle fracture^{9,10}. Moreover, high temperature flow mechanism of MGs can be a turning point for deep understanding of their plasticity in various conditions¹¹⁻¹³. For this purpose, there is a need to use a comprehensive model including various conditions.

Recently, researchers have tried to study the flow behavior of MGs at the atomic scale and defined deformation

mechanism based on free volumes, shear transformation zones or nanoscale flow units¹⁴⁻¹⁹. However, it seems that the physical-based models should be employed to evaluate the constitutive behavior of MGs under a workable situation. As an illustration, Rao et al.²⁰ developed a new two-leveled homogenization model by extending the traditional Mori-Tanaka's method for evaluating the failure evolution of MG composites under the monotonic uniaxial tensile and compressive loading conditions. In another work, a failure mechanism based constitutive model for bulk metallic glass was proposed, in which the nucleation and coalescence of nano-voids during the deformation was estimated²¹. Another study presented a thermodynamically constitutive model of MGs by extending an infinitesimal deformation approach, in which the multiplicative decomposition of deformation gradient and additive decomposition of free energy was considered²². Yao et al.²³ developed a size-dependent constitutive model of MGs and found that the size effect is a crucial factor in micro forming processes. Being able to apply for MGs, the Zener-Hollomon approach was considered by Yao et al.⁷,

*e-mail: tzuchiachen1688@gmail.com

in which the temperature effects and strain rate alterations are included in the model to evaluate the high temperature tensile deformation process. Hence, it is concluded that the determination of Zener-Hollomon parameters may lead to the identification of strain rate-temperature correlation in the deformation of MGs. In this work, we considered both experimental and theoretical aspects and estimated the Zener-Hollomon parameters to propose a criterion relating the stress flow, strain and temperature under a tensile loading.

Recently, the Si minor addition has been extensively investigated in the several alloying systems²⁴⁻²⁷. To provide some examples, Xue et al.²⁸ indicated that the Si microalloying in $Gd_{55}Co_{20}Al_{25}$ causes a more fragile liquid behavior and a smaller strength of liquid-liquid transition. Furthermore, the minor addition improves the formation of a nanocrystal-like structure frustrating the further growth of other crystal phases and stabilizes the glassy structure. Shao et al.²⁹ showed that the growth of crystalline phase is sluggish for $Dy_{55}Co_{20}Al_{24}Si_1$ amorphous alloy, associated with the interaction of kinetic fragility of super-cooled liquid and driving force for crystallization. Tsai et al.⁰ reported that the Si minor addition leads to a positive effect on promoting the GFA in the $Ti_{40}Zr_{10}Cu_{36}Pd_{14}$ alloy system. Using high resolution transmission electron microscopy (TEM), it was found that the Si triggers nano-crystalline phase formation in the glassy structure of $Cu_{60}Zr_{30}Ti_{10}$ ³¹. In another work, it was unveiled that the Si minor addition in a high entropy MG induces the competition between the crystal-like structures and the icosahedra-like clusters and promotes the creation of stable network structure, inhibiting the crystallization in the material³². To clearly show the alloying composition effects, we also considered a novel MG composition ZrCoAl(Si), in which the Si addition leads to the improvement of glass forming ability (GFA) in the amorphous system³³. Our eventual aim is to indicate that how Si minor addition in the chemical composition affects the flow stress characteristics of the Zr-based MG.

2. Materials and Methods

Using high purity elements, master alloys with chemical compositions of $Zr_{60}Co_{34}Al_6$ and $(Zr_{60}Co_{34}Al_6)_{97}Si_3$ were prepared by arc re-melting process under vacuum of 10^{-4} Torr. The master alloys were re-melted five times for elemental homogeneity. The prepared ingots were then cast by melt spinning technique in the form of ribbons with thickness of 32 μ m and 4 mm width. X-ray diffraction (XRD) was performed to ensure the amorphous nature of ribbons. Moreover, differential scanning calorimetry (DSC) test with heating rate of 20 K/min under Ar environment was done to measure the thermal properties of MG ribbons (see Figure 1). For evaluation of flow behavior of MG ribbons at high temperatures, GABO EPLEXOR instrument was used to measure the tensile strain rate jump features of MG ribbons under the dynamic mechanical analysis (DMA) mode. For this purpose, the test was carried out under different strain rates and temperature of 0.96, 1 and 1.04 T_g . For each strain rate, the MG ribbon was held for 2 min at each step to ensure the exact flow stress measurement in each state and then a jump to the higher strain rates was done (see Figure 2).

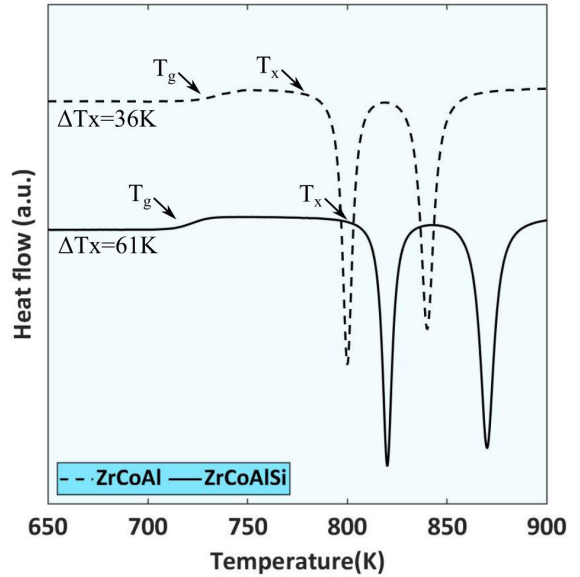


Figure 1. DSC curves of ZrCoAl and ZrCoAlSi MGs at a) T_g and T_x regions b) liquidus region.

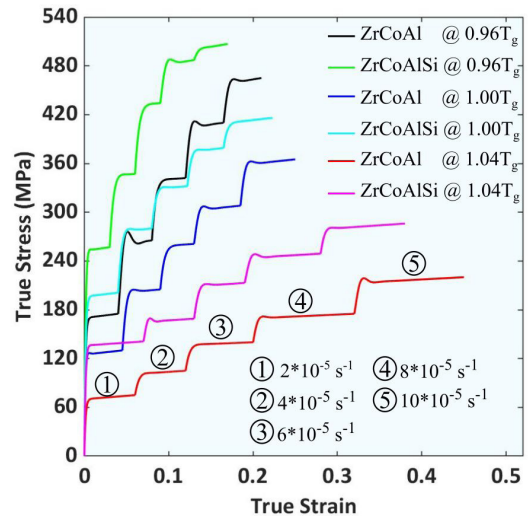


Figure 2. The stress-strain curves of ZrCoAl and ZrCoAlSi MGs obtained from strain-rate jump test under different temperatures.

3. Results and Discussion

The DSC curves of ZrCoAl and ZrCoAlSi MG samples from 650 K up to 1250 K are presented in Figure 1. As observed, the Si minor addition increases the temperature of crystallization events (T_x); however, a slight decrement was also detected in the T_g value. Moreover, one can see that the liquidus temperature (T_l) was declined in the ZrCoAlSi MG sample. This result shows that the Si element leads to the improvement of thermal stability and GFA in the Zr-based MG. Wang³⁴ indicated that the betterment of thermal stability under the microalloying process depends on the two main factors. First of all, the selected atom should be

small enough to enhance the density of randomly packed arrangements in the liquid. Secondly, the added atoms should lower the melting point for stabilizing of the liquid phase. In this work, the Si minor addition perfectly plays the role of a proper trace element declining the melting point and stabilizing the liquid phase in the alloying composition. In previous works, it is also reported that the Si addition in the ZrCoAl system produces the short range order (SRO) clusters with low coordination number (CN=9), which is compatible with interstitial space occupation of the small-size Si atoms³³. Consequently, the variety of clusters increases in the alloying system and the thermodynamically liquid stabilization occurs with respect to competing crystalline phases. It should be noted that the smaller difference between T_g and T_p , detected in the Si-added sample, favors the glass formation, because it needs lower cooling rates to inhibit crystalline nucleation during solidification²⁷. Furthermore, a large negative heat of mixing in the Si-Zr (-84 kJ/mol), Si-Co (-38 kJ/mol) and Si-Al (-16 kJ/mol) pairs is another factor expecting the high GFA and liquid stability in the ZrCoAlSi alloy³³.

Figure 2 illustrates the stress-strain curves of MG ribbons under a strain rate jump trend at 0.96, 1, 1.04 T_g . As observed, both of MG ribbons showed stable flow stress at low strain rates. It is also seen that the lower strain rate is accompanied with the lower flow stress. On the other side, the increase in strain rate leads to an enhancement (overshoot) in flow stresses. However, the enhancement strongly depends on the temperature and alloying composition. According to the literature, the stable part of curves, i.e. at low strain rates, shows that the flow stress is associated to the free volume dynamics^{7,35}. According to the free volume theory, the induced stress leads to the annihilation of short and medium range scale clusters and provides more disordered structures, which is corresponding to the small strains. At higher strain rates, in which high flow stress levels are observed, the induced strain is related to the formation and percolation of shear transformation zones (STZs) governing the plasticity behavior of amorphous alloys^{36,37}. Considering alloying composition, it is clear that the Si microalloying leads to a delay in the enhancement of flow stress in all the tested temperatures. This means that the minor addition improves the homogenized plasticity in the material and accelerates the formation and distribution of STZs in the structure. Hence, the sudden enhancement of flow stress is postponed.

To quantitatively analyze the flow stress trend in a high temperature deformation process, it is required to extract the inherent materials properties from incorporating the experimentations and constitutive approaches. In general, it is plausible to relate the strain rate, temperature and stable flow stress magnitude using Arrhenius function. The Zener-Hollomon approach should be considered for high temperature deformation (i.e. near T_g). Using the following equation as a general model, one can correlate the Zener-Hollomon parameter (Z) and flow stress magnitude^{38,39}:

$$Z = \dot{\epsilon} \exp\left(\frac{Q}{RT}\right) = A [\sinh(\alpha\sigma)]^n = A\sigma^n \quad (1)$$

Where $\dot{\epsilon}$ and Q are strain rate and activation energy for high temperature deformation, respectively. T and R define temperature and gas constant. Flow stress is introduced by σ , while n , A and $\alpha=\beta/n'$ are materials constants. For measuring the flow stress, it is necessary to obtain the constants and the inherent materials properties. Based on the mentioned equation, the inclines of $\ln \dot{\epsilon}$ vs. σ and $\ln \dot{\epsilon}$ vs. $\ln \sigma$ can determine the values of β and n' , respectively. Consequently one can calculate α constant using β and n' . Figure 3a-d shows the fitting of $\ln \dot{\epsilon}$ - σ and $\ln \dot{\epsilon}$ - $\ln \sigma$ curves at different temperatures. According to the results, with the increase in temperature, the incline of $\ln \dot{\epsilon}$ - $\ln \sigma$ curves decreases, showing the slight decline in β value. On the other side, the increase in temperature leads to the incline enhancement of $\ln \dot{\epsilon}$ - σ curves, which indicates the increase of n' value. Considering Table 1, it is concluded that both samples are affected by the temperature so that α constant decreases at higher temperatures. It is also found that α sensitivity is much higher in Si-free samples, which may be due to the lower thermal stability in this sample.

Using Equation 2, the activation energy (Q) can be calculated for high temperature situation⁷:

$$Q = R \left[\frac{\partial \ln \dot{\epsilon}'}{\partial \ln(\sinh(\alpha\sigma))} \right] \left[\frac{\partial \ln(\sinh(\alpha\sigma))}{\partial (1/T)} \right] \quad (2)$$

Considering the mentioned equation and fitting the curves of $\ln \dot{\epsilon}$ vs. $\ln [\sinh(\alpha\sigma)]$, it is possible to averagely calculate the n value in a stable flow stress situation (see Figure 4). The average n value in our work is 0.72 and 0.69 for Si-free and Si-added samples, respectively, which is slightly lower than that calculated in other works^{7,40}. With the evaluation of inclines of $1/T$ vs. $\ln [\sinh(\alpha\sigma)]$ curves, one can estimate the activation energy (Q), which is in the range of 276 KJ/mol and 281 KJ/mol for Si-free and Si-added samples, respectively. As illustrated in Figure 4, again it is clear that the Si-added sample is less sensitive to any external factor such as temperature. In the next step, with the insertion of mean Q and other attained constants into Equation 1, Z parameter can be estimated. Moreover, the incorporation of Equation 1 and 2 can give the $\ln Z$ vs. $\ln [\sinh(\alpha\sigma)]$ curves and constants A and n can be obtained from the fitted curves, as given in Figure 5 and Table 1. According to the fitted curves, the linear regression is 98.5% and 99% for our samples, showing the high reliability of results. Now based on Equation 1, it is conceivable to establish a constitutive equation describing the correlation between flow stress and strain rate in a selected temperature for our samples:

$$\dot{\epsilon}' = (1.31 \times 10^{25}) [\sinh(0.0143\sigma)]^{0.72} \exp\left(-\frac{276000}{RT}\right) \quad (3)$$

Table 1. Intrinsic features of MGs.

	$\alpha_{(0.96T_g)}$	$\alpha_{(1T_g)}$	$\alpha_{(1.04T_g)}$	$\alpha_{ave.}$	$n_{ave.}$	$Q_{ave.}$	A
ZrCoAl	0.011	0.014	0.018	0.0143	0.72	276	1.31×10^{25}
ZrCoAlSi	0.015	0.016	0.019	0.0166	0.67	281	1.98×10^{25}

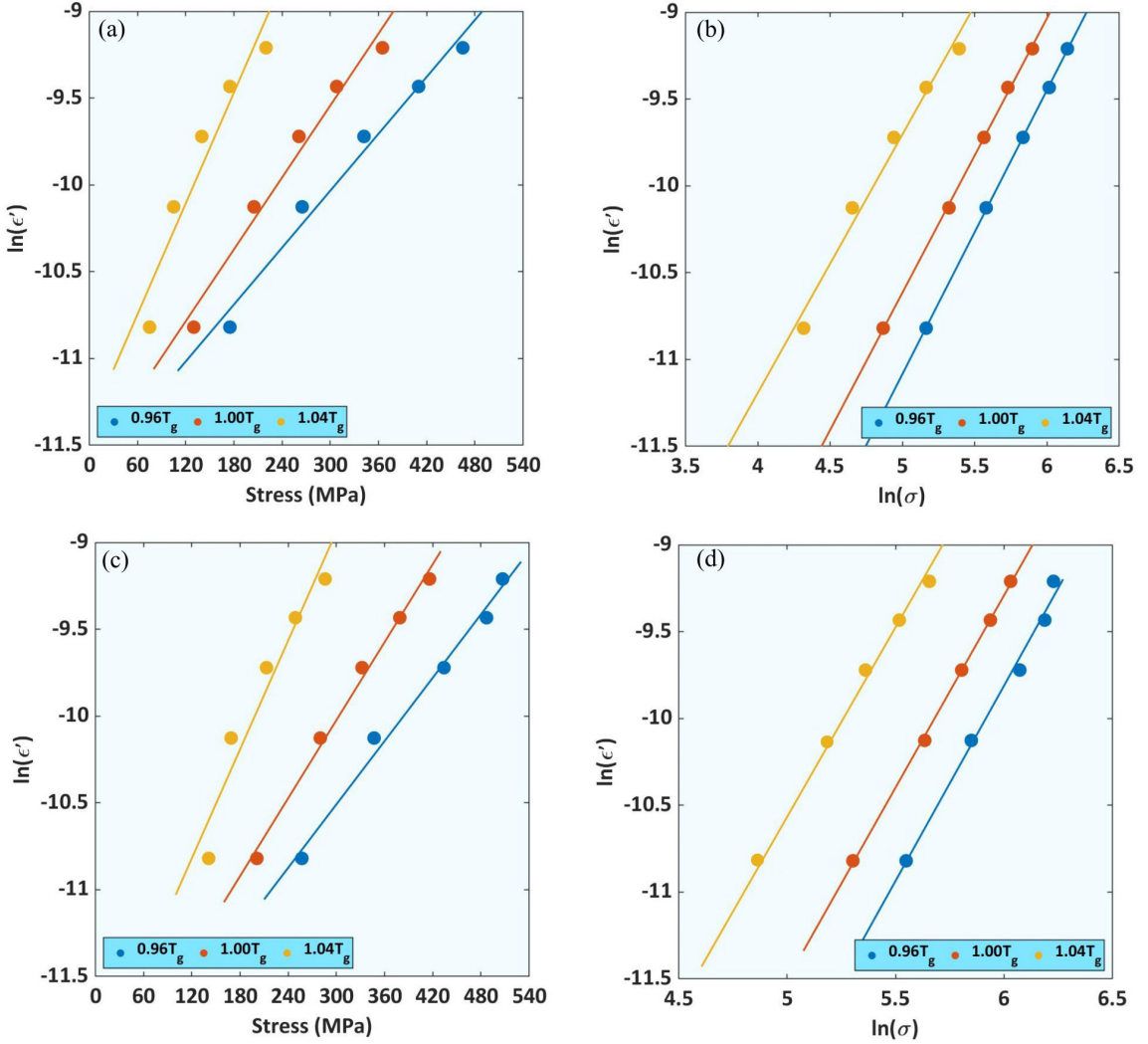


Figure 3. Fitting of a) $\ln \dot{\epsilon}$ - σ curve for ZrCoAl, b) $\ln \dot{\epsilon}$ - $\ln \sigma$ curve for ZrCoAl, c) $\ln \dot{\epsilon}$ - σ curve for ZrCoAlSi, d) $\ln \dot{\epsilon}$ - $\ln \sigma$ curve for ZrCoAlSi at different temperatures.

$$\dot{\epsilon}' = \left(1.98 \times 10^{25}\right) \left[\sinh(0.0166\sigma)\right]^{0.67} \exp\left(-\frac{281000}{RT}\right) \quad (4)$$

Now it is credible to interpret the high temperature deformation of MGs based on the free volume theory. As free volume point of view, the true flow stress, temperature and free volume content strongly depend on the strain rate in the hot deformation processing situation³⁶:

$$\dot{\epsilon} = \dot{\epsilon}_0 \sinh\left(\frac{\sigma V}{2(3^{1.2})KT}\right) \quad (5)$$

In which T and K are temperature and Boltzmann constant, respectively. $\dot{\epsilon}_0$ introduces the frequency factor and V is the activation volume. Knowing the flow stress and the strain rate, the viscosity can be obtained from the following equation:

$$\eta = \frac{\sigma}{3\dot{\epsilon}} \quad (6)$$

Considering Equations 5 and 6, one can estimate the frequency factor, the activation volume and the viscosity in different temperatures. Moreover, the average size of a flow unit can be obtained by $V = \gamma \cdot \phi$; in which γ indicates the local shear strain ($=0.125^{41}$) and ϕ is flow unit sizes (see Table 2). Figure 6 shows the viscosity as a function of temperature in both of MG samples. As observed, the variations of viscosity as a function of temperature in the Si-added sample is more uniform than the Si-free one. Moreover, sharper viscosity changes happen in the Si-free sample showing the premature overshoots, which was observed in the flow stress changes, given in Figure 2. On the other side, the average flow unit sizes in the Si-added sample is lower than the Si-free one (see Table 2). It is worth-mentioning that the ϕ value just indicates the average flow unit sizes and is not consistent with the degree of disordering in the glassy structure. In other words, one glassy structure (such as our Si-added sample) comprises numerous homogeneous flow units with averagely small sizes and another glassy structure (such as

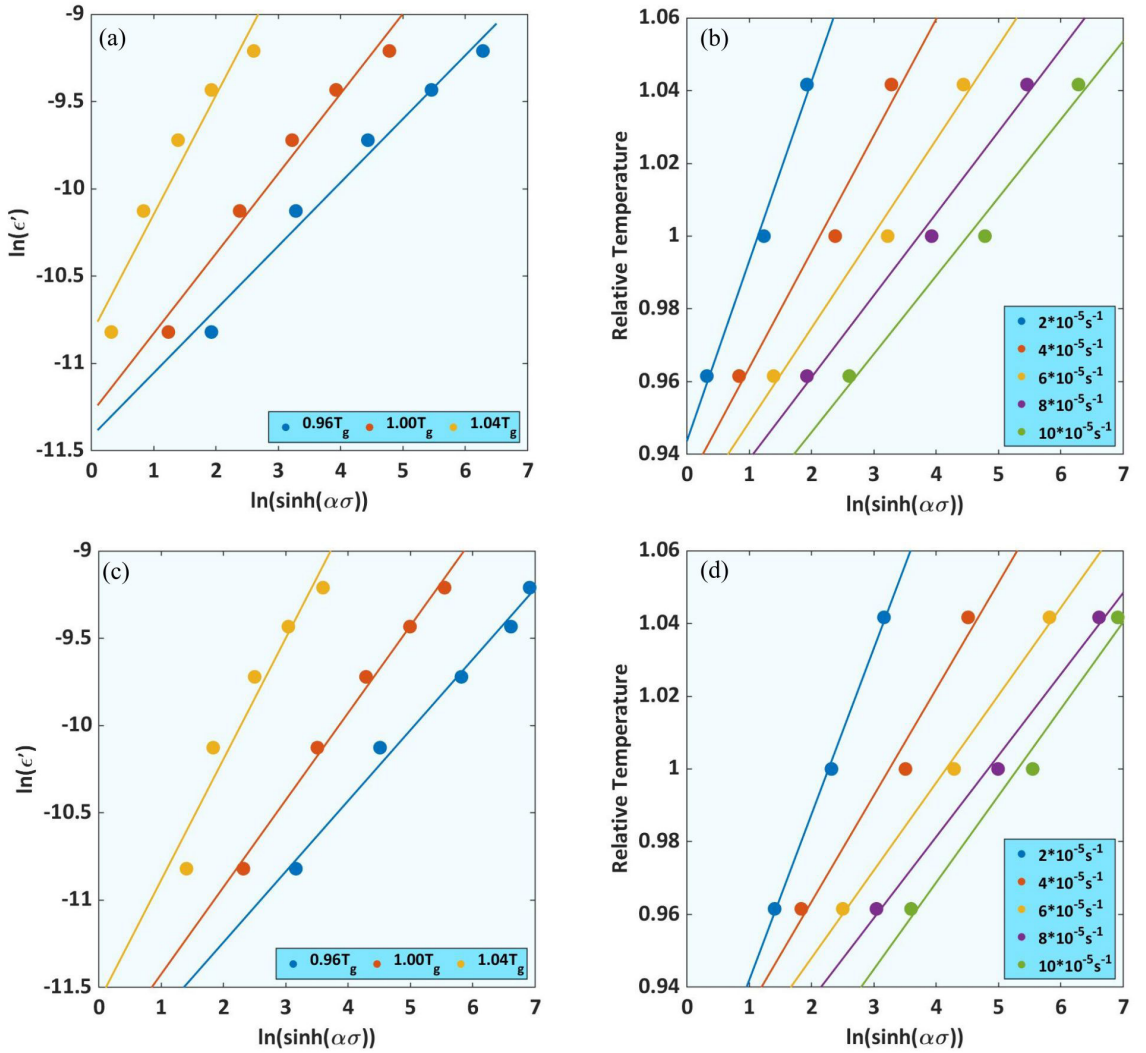


Figure 4. Fitting of a) $\ln \dot{\epsilon}$ vs. $\ln [\sinh(\alpha\sigma)]$ curve for ZrCoAl, b) $1/T$ vs. $\ln [\sinh(\alpha\sigma)]$ curve for ZrCoAl, c) $\ln \dot{\epsilon}$ vs. $\ln [\sinh(\alpha\sigma)]$ curve for ZrCoAlSi, d) $1/T$ vs. $\ln [\sinh(\alpha\sigma)]$ curve for ZrCoAlSi at different temperatures.

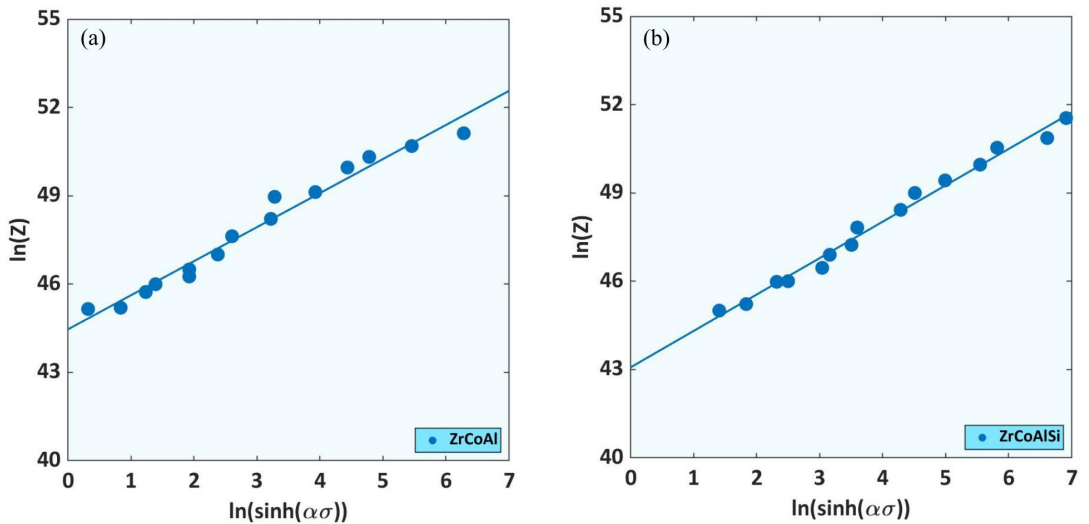
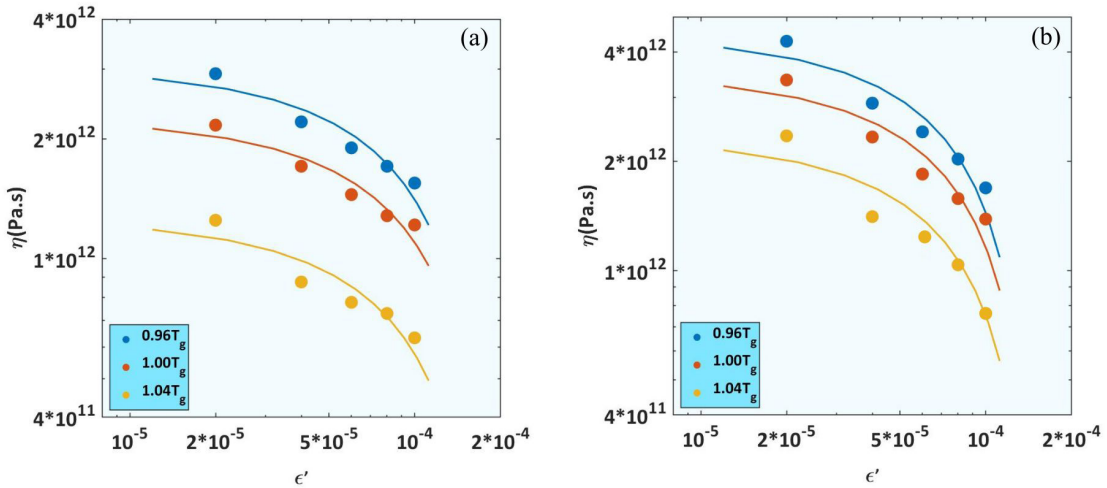


Figure 5. Fitted values of Zener-Hollomon parameter ($\ln Z$) vs. flow stress for a) ZrCoAl, b) ZrCoAlSi.

Table 2. Free volume size, activation volume (nm^3) and frequency factor (S^{-1}) of ZrCoAl and ZrCoAlSi MGs.

	$V_{(0.96T_g)}$	$V_{(1T_g)}$	$V_{(1.04T_g)}$	$\mathcal{E}_{0(0.96T_g)}$	$\mathcal{E}_{0(1T_g)}$	$\mathcal{E}_{0(1.04T_g)}$	$\Phi_{\text{ave.}}$
ZrCoAl	0.173	0.291	0.478	2.31×10^{-5}	2.93×10^{-5}	3.21×10^{-5}	3.335
ZrCoAlSi	0.139	0.218	0.391	2.19×10^{-5}	2.39×10^{-5}	2.55×10^{-5}	2.514

**Figure 6.** Viscosity as a function of strain rate in a) ZrCoAl, b) ZrCoAlSi.

our Si-free sample) includes lower flow units with bigger size. Many works, done by researchers, have showed that the homogeneous plasticity in the MGs relies on the homogenous structural characterization such as uniform distribution of flow units^{42,43}. Hence, one can see that the Si-added MG sample shows delayed enhancement, i.e. overshoot, at the higher strain rates. This was due to the fact that the Si atoms with small size lead to the formation of small atomic clusters in the glassy structure and improves the elemental and configurational heterogeneity in the material³³. This result agrees with other works focusing on the plasticity and viscoplastic behavior of microalloyed MGs. To provide some detailed examples, it was unveiled that the minor addition into the CuZr systems leads to the increase in the yield strength and plastic strain, so that the work hardening was also detected under the compressive test³⁴. It was suggested that the microalloying process induced the individual structure correlated with the atomic-scale heterogeneities increasing the potential of extensive shear band formation. This result is consistent with our work, in which the Si addition controls the sudden stress overshoots and strain increment in the MG. Moreover, it was observed that the viscosity behavior with the increase in the strain rate and temperature is more stable in the Si-added sample, showing the high capability of viscoplastic response in this state. As depicted in other works, if the minor addition causes the higher thermal stability in the super-cooled liquid, the viscoplastic response improves, which is due to the homogeneous generation of loosely packed structure in the structure^{44,45}. Consequently, it is derived that the minor addition with a negative heat of mixing and a proper size can amend the thermal stability, GFA and homogenous flow characteristics of MG alloys.

4. Conclusions

In this work, the DSC experiment and the strain rate jump test were carried out to reveal the role Si minor addition on the thermal behavior and the flow stress characteristics of ZrCoAl(Si) MGs. Using DSC analysis, it was found that the Si microalloying process leads to the significant improvement of thermal stability and GFA in the Zr-based MG. This event is owing to the small size of Si atom inducing the formation of denser atomic structures and liquid stabilization in the system. Zener-Hollomon approach was employed to define the strain rate sensitivity when the Si element was added into the ZrCoAl amorphous system. Under a wide range of applied strain rate and temperature, the activation energy of 276 and 281 kJ/mol and exponent of 0.72 and 0.67 were calculated for the ZrCoAl and ZrCoAlSi MGs, respectively. This result showed that the Si microalloying process stabilizes the flow stress characteristics in temperatures around T_g and decreases the sensitivity to the strain rate. It was also detected that the viscosity behavior in the Si-added sample is less sensitive to the strain rate, indicating the high capability of viscoplastic response in the ZrCoAlSi alloy.

5. References

1. Poddar C, Jayaraj J, Amirthapandian S, Ningshen S. Effect of thermally grown amorphous oxide film on the corrosion resistance properties of Ni50Zr25Nb25 metallic glass in nitric acid medium. *Intermetallics*. 2019;113:106571. <http://dx.doi.org/10.1016/j.intermet.2019.106571>.
2. Hua N, Zhang X, Liao Z, Hong X, Guo Q, Huang Y, et al. Dry wear behavior and mechanism of a Fe-based bulk metallic glass: description by Hertzian contact calculation and finite-element method simulation. *J Non-Cryst Solids*. 2020;543:120065. <http://dx.doi.org/10.1016/j.jnoncrsol.2020.120065>.

3. Yamada R, Shibazaki Y, Abe Y, Ryu W, Saida J. Unveiling a new type of ultradense anomalous metallic glass with improved strength and ductility through a high-pressure heat treatment. *NPG Asia Mater.* 2019;11:72. <http://dx.doi.org/10.1038/s41427-019-0175-1>.
4. Guo H, Yan PF, Wang YB, Tan J, Zhang ZF, Sui ML, et al. Tensile ductility and necking of metallic glass. *Nat Mater.* 2007;6:735-9. <http://dx.doi.org/10.1038/nmat1984>.
5. Zhang ZF, Eckert J, Schultz L. Difference in compressive and tensile fracture mechanisms of Zr₅₉Cu₂₀Al₁₀Ni₈Ti₃ bulk metallic glass. *Acta Mater.* 2003;51:1167-79. [http://dx.doi.org/10.1016/S1359-6454\(02\)00521-9](http://dx.doi.org/10.1016/S1359-6454(02)00521-9).
6. Viswanathan K, Yadav S, Sagapuram D. Shear banding and fracture in large strain deformation: understanding the mechanics of flow localization from Zener's time to the present. *ArXiv Prepr.* 2020;arXiv:2007.01798v3.
7. Yao ZF, Qiao JC, Pelletier JM, Yao Y. Effect of Zener-Hollomon parameter on the flow behavior of Zr-based metallic glass. *J Alloys Compd.* 2020;819:152987. <http://dx.doi.org/10.1016/j.jallcom.2019.152987>.
8. Jiang Y. Micromechanics constitutive model for predicting the stress-strain relations of particle toughened bulk metallic glass matrix composites. *Intermetallics.* 2017;90:147-51. <http://dx.doi.org/10.1016/j.intermet.2017.07.015>.
9. Jiang Y. Mesoscopic constitutive model for predicting failure of bulk metallic glass composites based on the free-volume model. *Materials (Basel).* 2018;11(2):327.
10. Rao W, Zhang J, Jiang H, Kang G. Meso-mechanical constitutive model of bulk metallic glass matrix composites. *Mech Mater.* 2016;103:68-77. <http://dx.doi.org/10.1016/j.mechmat.2016.09.008>.
11. Song SM, Liao YC, Li TH, Lee CK, Tsai PH, Jang JSC, et al. Thermoplastic deformation behavior of a Fe-based bulk metallic glass within the supercooled liquid region. *J Mater Res Technol.* 2019;8:1907-14. <http://dx.doi.org/10.1016/j.jmrt.2019.01.007>.
12. Qiao JC, Pelletier JM, Yao Y. Creep in bulk metallic glasses. Transition from linear to non linear regime. *Mater Sci Eng A.* 2019;743:185-9. <http://dx.doi.org/10.1016/j.msea.2018.11.066>.
13. Chen Y, Qiao J. Correlation between high temperature deformation and β relaxation in LaCe-based metallic glass. *Materials (Basel).* 2020;13:833.
14. Şopu D, Moitzi F, Mousseau N, Eckert J. An atomic-level perspective of shear band formation and interaction in monolithic metallic glasses. *Appl. Mater. Today.* 2020;21:100828. <http://dx.doi.org/10.1016/j.apmt.2020.100828>.
15. Zhang Q, Li Q-K, Zhao S-F, Wang W-H, Li M. Structural characteristics in deformation mechanism transformation in nanoscale metallic glasses. *J Phys Condens Matter.* 2019;31:455401.
16. Dong F, He M, Zhang Y, Wang B, Luo L, Su Y, et al. Investigation of shear transformation zone and ductility of Zr-based bulk metallic glass after plasma-assisted hydrogenation. *Mater Sci Eng A.* 2019;759:105-11. <http://dx.doi.org/10.1016/j.msea.2019.05.027>.
17. Geng K, Yang W, Mo J, Liu H, Wei F, Ma Z, et al. Plastic deformation mechanism of ductile Fe₅₀Ni₃₀P₁₃C₇ metallic glass. *Met Mater Int.* 2019;25:487-98. <http://dx.doi.org/10.1007/s12540-018-0181-9>.
18. Fu WJ, Zheng W, Axinte E, Huang YJ, Lee TL, Li HG, et al. Tensile deformation mechanism of a bulk metallic glass matrix composite using in situ neutron diffraction. *J Non-Cryst Solids.* 2020;546:120267. <http://dx.doi.org/10.1016/j.jnoncrysol.2020.120267>.
19. Samavatian M, Gholamipour R, Amadeh AA, Mirdamadi S. Role of tensile elastostatic loading on atomic structure and mechanical properties of Zr₅₅Cu₃₀Ni₅Al₁₀ bulk metallic glass. *Mater Sci Eng A.* 2019;753:218-23. <http://dx.doi.org/10.1016/j.msea.2019.03.058>.
20. Rao W, Zhang J, Kang G, Yu C, Jiang H. A meso-mechanical constitutive model of bulk metallic glass composites considering the local failure of matrix. *Int J Plast.* 2019;115:238-67. <http://dx.doi.org/10.1016/j.ijplas.2018.11.017>.
21. Rao W, Zhang J, Kang G. A failure mechanism based constitutive model for bulk metallic glass. *Mech Mater.* 2018;125:52-69. <http://dx.doi.org/10.1016/j.mechmat.2018.07.005>.
22. Viswanathan K, Yadav S, Sagapuram D. Shear bands in materials processing: understanding the mechanics of flow localization from zener's time to the present. *Appl Mech Rev.* 2020;72(6):060802.
23. Yao D, Deng L, Zhang M, Wang X, Tang N, Li J. A size-dependent constitutive model of bulk metallic glasses in the supercooled liquid region. *Sci Rep.* 2015;5:8083. <http://dx.doi.org/10.1038/srep08083>.
24. Zhang T, Men H, Pang SJ, Fu JY, Ma CL, Inoue A. Effects of a minor addition of Cu-Zr-Ti bulk metallic glass. *Mater Sci Eng A.* 2007;449-451:295-8. <http://dx.doi.org/10.1016/j.msea.2005.12.102>.
25. Gargarella P, Pauly S, Khoshkhoo MS, Kiminami CS, Kühn U, Eckert J. Improving the glass-forming ability and plasticity of a TiCu-based bulk metallic glass composite by minor additions of Si. *J Alloys Compd.* 2016;663:531-9. <http://dx.doi.org/10.1016/j.jallcom.2015.12.160>.
26. Chen N, Louzguine-Luzgin DV, Xie GQ, Wada T, Inoue A. Influence of minor Si addition on the glass-forming ability and mechanical properties of Pd₄₀Ni₄₀P₂₀ alloy. *Acta Mater.* 2009;57:2775-80. <http://dx.doi.org/10.1016/j.actamat.2009.02.028>.
27. Yazici ZO, Hitit A, Yalcin Y, Ozgul M. Effects of minor Cu and Si additions on glass forming ability and mechanical properties of Co-Fe-Ta-B Bulk metallic glass. *Met Mater Int.* 2016;22:50-7. <http://dx.doi.org/10.1007/s12540-016-5220-9>.
28. Xue L, Shao L, Luo Q, Hu L, Zhao Y, Yin K, et al. Liquid dynamics and glass formation of Gd₅₅Co₂₀Al₂₅ metallic glass with minor Si addition. *J Mater Sci Technol.* 2021;77:28-37. <http://dx.doi.org/10.1016/j.jmst.2020.11.024>.
29. Shao L, Xue L, Wang Q, Ma K, Huang J, Shen B. Effects of Si addition on glass-forming ability and crystallization behavior of DyCoAl bulk metallic glass. *J Alloys Compd.* 2021;874:159964. <http://dx.doi.org/10.1016/j.jallcom.2021.159964>.
30. Tsai PH, Hsu KT, Ke JH, Lin HC, Jang JSC, Huang JC. Microalloying effect of Si on mechanical properties of Ti based bulk metallic glass. *Mater Technol.* 2015;30:161-5. <http://dx.doi.org/10.1179/17535557A15Y.000000003>.
31. Fan GJ, Fu LF, Qiao DC, Choo H, Liaw PK, Browning ND, et al. Effect of microalloying on the glass-forming ability of Cu₆₀Zr₃₀Ti₁₀ bulk metallic glass. *J Non-Cryst Solids.* 2007;353:4218-22. <http://dx.doi.org/10.1016/j.jnoncrysol.2007.08.057>.
32. Shao L, Wang Q, Xue L, Zhu M, Wang A, Luan J, et al. Effects of minor Si addition on structural heterogeneity and glass formation of GdDyErCoAl high-entropy bulk metallic glass. *J Mater Res Technol.* 2021;11:378-91. <http://dx.doi.org/10.1016/j.jmrt.2021.01.035>.
33. Samavatian M, Gholamipour R, Samavatian V. Discovery of novel quaternary bulk metallic glasses using a developed correlation-based neural network approach. *Comput Mater Sci.* 2021;186:110025. <http://dx.doi.org/10.1016/j.commatsci.2020.110025>.
34. Wang WH. Roles of minor additions in formation and properties of bulk metallic glasses. *Prog Mater Sci.* 2007;52:540-96. <http://dx.doi.org/10.1016/j.pmatsci.2006.07.003>.
35. Jiang MQ, Wilde G, Dai LH. Origin of stress overshoot in amorphous solids. *Mech Mater.* 2015;81:72-83. <http://dx.doi.org/10.1016/j.mechmat.2014.10.002>.
36. Yao ZF, Qiao JC, Pelletier JM, Yao Y. High temperature deformation behaviors of the Zr_{63.36}Cu_{14.57}Ni_{10.12}Al₁₂ bulk metallic glass. *J Mater Sci.* 2016;51:4079-87. <http://dx.doi.org/10.1007/s10853-016-9729-6>.
37. Qiao JC, Wang Y-J, Pelletier JM, Keer LM, Fine ME, Yao Y. Characteristics of stress relaxation kinetics of La₆₀Ni₁₅Al₂₅

- bulk metallic glass. *Acta Mater.* 2015;98:43-50. <http://dx.doi.org/10.1016/j.actamat.2015.07.020>.
38. Mirzadeh H. Constitutive analysis of Mg–Al–Zn magnesium alloys during hot deformation. *Mech Mater.* 2014;77:80-5. <http://dx.doi.org/10.1016/j.mechmat.2014.07.004>.
 39. Tang Y, Guo X. High temperature deformation behavior of an optimized Nb–Si based ultrahigh temperature alloy. *Scr Mater.* 2016;116:16-20. <http://dx.doi.org/10.1016/j.scriptamat.2016.01.033>.
 40. Gun B, Laws KJ, Ferry M. Superplastic flow of a Mg-based bulk metallic glass in the supercooled liquid region. *J Non-Cryst Solids.* 2006;352:3896-902. <http://dx.doi.org/10.1016/j.jnoncrysol.2006.06.023>.
 41. Qiao JC, Pelletier JM. Enthalpy relaxation in $\text{Cu}_{46}\text{Zr}_{45}\text{Al}_7\text{Y}_2$ and $\text{Zr}_{55}\text{Cu}_{30}\text{Ni}_5\text{Al}_{10}$ bulk metallic glasses by differential scanning calorimetry (DSC). *Intermetallics.* 2011;19:9-18. <http://dx.doi.org/10.1016/j.intermet.2010.08.042>.
 42. Kosiba K, Şopu D, Scudino S, Zhang L, Bednarcik J, Pauly S. Modulating heterogeneity and plasticity in bulk metallic glasses: role of interfaces on shear banding. *Int J Plast.* 2019;119:156-70. <http://dx.doi.org/10.1016/j.ijplas.2019.03.007>.
 43. Gao M, Dong J, Huan Y, Wang YT, Wang W-H. Macroscopic tensile plasticity by scalarizing stress distribution in bulk metallic glass. *Sci Rep.* 2016;6:21929. <http://dx.doi.org/10.1038/srep21929>.
 44. Kim YJ, Kim JS, Kim WC, Park JW, Kim WT, Kim DH. Effect of Al addition on thermal stability and thermoplastic forming ability of $\text{Ti}_{35}\text{Zr}_{15}\text{Ni}_{40}\text{Cu}_{10}$ metallic glass in the supercooled liquid region. *Met Mater Int.* 2021. <http://dx.doi.org/10.1007/s12540-021-00989-6>.
 45. Yuan CC, Lv ZW, Pang CM, Zhu WW, Wang X-L, Shen BL. Pronounced nanoindentation creep deformation in Cu-doped CoFe-based metallic glasses. *J Alloys Compd.* 2019;806:246-53. <http://dx.doi.org/10.1016/j.jallcom.2019.07.226>.